Modeling of Mass Transport in 3D Vascularized Porous Tissue Scaffolds

Xuan Mu[1], David L. Kaplan[1]
1. Department of Biomedical Engineering, Tufts University, Medford, MA 02155, USA

INTRODUCTION: Geometric characteristics of a vascularized porous scaffold, such as pore size and embedded channels, are important design parameters.[1] However, conventional computational simulations are usually based on either a single or parallel straight channels[2], which is over-simplified in comparison to the curved and entangled morphologies found either in nature or in 3D printed vasculature[3], for example, entangled straight and helix channels and mathematical space-filling Hilbert curves (Figure 1). Here, we employed the CFD module of COMSOL Multiphysics® 5.4 to investigate the influence of geometric parameters on mass transport of oxygen within the scaffold.

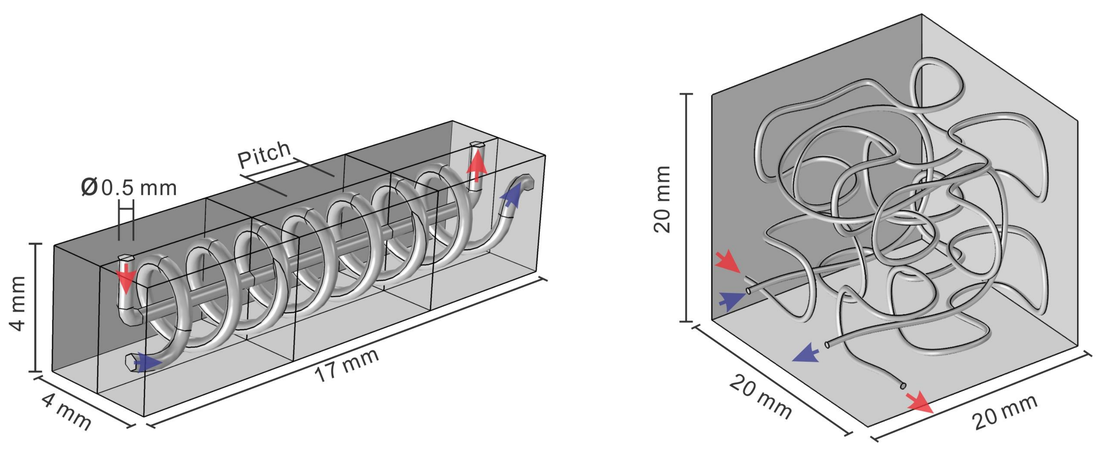

Figure 1. Two models of vascularized 3D porous scaffolds. Only channels and 3 boundary surface are displayed for clarity. The left one Is composed of a straight channel and a helix channel; the right one consists two Hilbert curves of one and two degrees, respectively. Arrows indicate the Inlets and outlets. Red and blue indicate independent channels.

COMPUTATIONAL METHODS: The flow in the vasculature and the bulk porous region is described by Navier-Stokes equations (1) and Forcheheimer-corrected Brinkman (2),

$$\rho(u\cdot\nabla)u = -\nabla\cdot\left[-\tau + \mathrm{P}\delta_{\mathrm{ij}}\right] \quad (1)$$

$$\nabla p = \mu\nabla^2 u_{\mathrm{s}} - \frac{\mu}{k}u_{\mathrm{s}} \quad (2)$$

where u is the velocity vector (m/s), τ is the dynamic viscosity (Pa·s), ρ is the fluid's density (kg/m^3), P is the pressure (Pa), δij is the Kronecker delta function, k is the permeability of the porous medium (m^2), u_s denotes the fluid superficial velocity vector (m/s), and μ is the effective viscosity in the porous medium (kg/m·s).

The combination of Fick's law and Michaelis-Menten reaction (3) is used to describe the concentration profile of oxygen and nutrients inside tissue scaffolds,

$$\nabla\cdot(-\mathrm{D}\nabla c) + \mathrm{u}\cdot\nabla c = -\frac{\mathrm{v_m}c}{\mathrm{k_m}+c}\mathrm{f}(c > c_{\mathrm{cr}}) \quad (3)$$

where c is the oxygen concentration (mol/m3), D is the oxygen diffusivity (3×10^{-9} m2/s), u is the velocity vector (m/s), v_m is the maximum reaction rate, km is the Michaelis constant, f is a smoothed Heaviside function, and c_{cr} critical concentration.

RESULTS: We simulated oxygen profile in a vascularized porous scaffold of straight-helix channels (Figure 2 and 3). The simulation encompasses a wide range of permeability and porosity that covers most, if not all, 3D printing and porous materials in the field of tissue engineering. Generally, smaller permeability and porosity lead to longer diffusion time. Under a certain inlet velocity, the influence of porosity and permeability is asymptotic. Moreover, the 3D profile of simulation demonstrates spatial distribution and explicitly indicates specific areas where the efficiency of mass transfer is limited and thus can be revised, if needed.

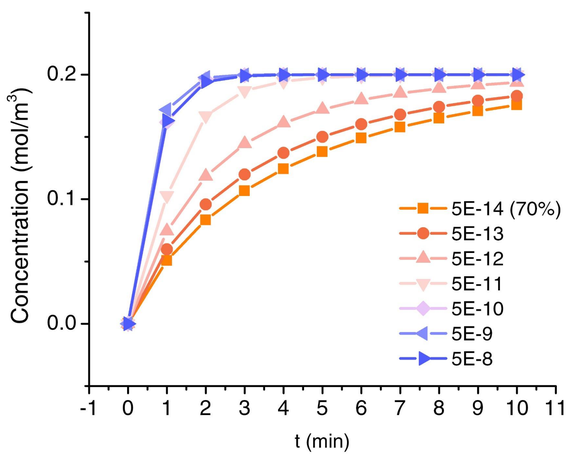

Figure 2. Averaged volume concentration of oxygen as a function of perfusion time under different permeabilities. Porosity is 70%.

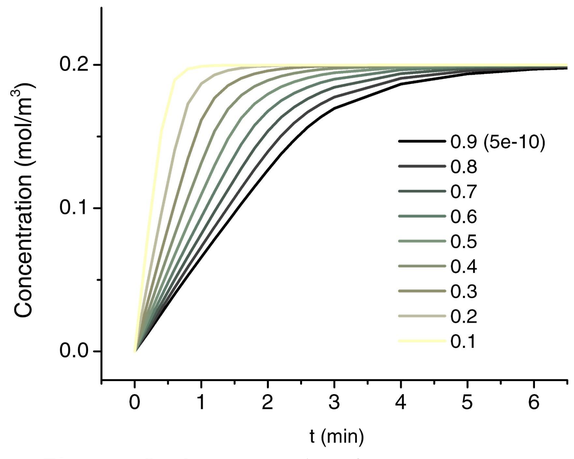

Figure 3. Averaged volume concentration of oxygen as a function of perfusion time under different porosities. Permeability is 5e-10 m^2.

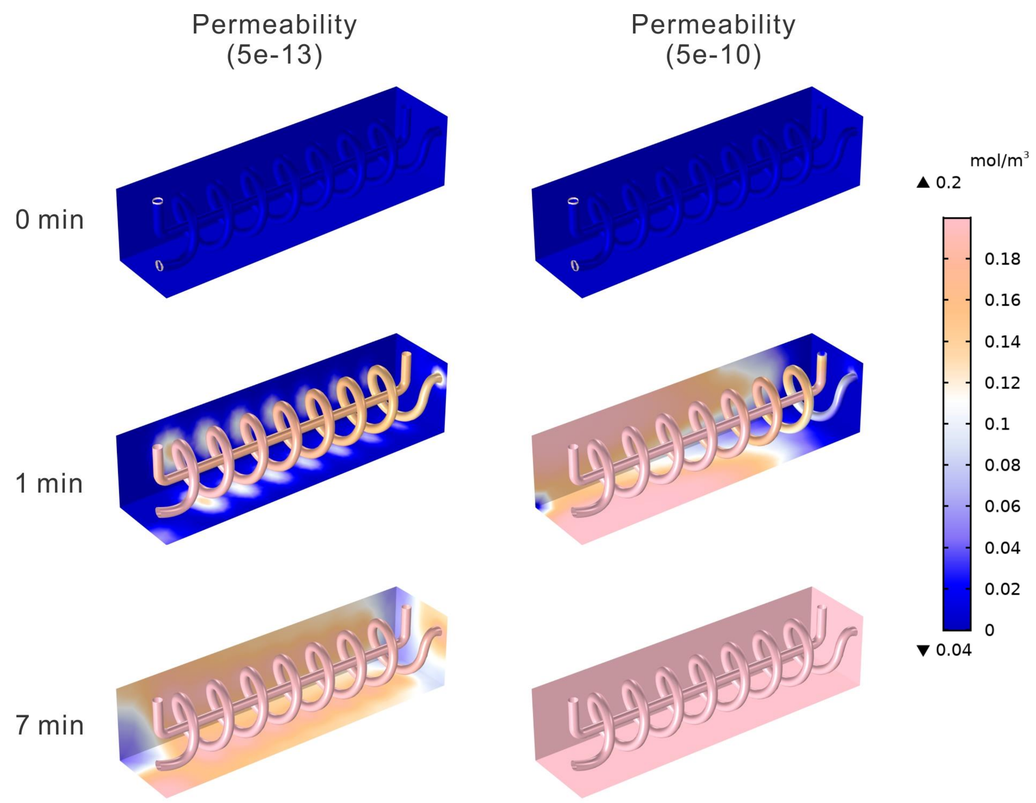

Figure 4. Comparison of 3D oxygen profile under different permeabilities.

CONCLUSIONS: Although the current simulation only focuses on the acellular scaffold of helix-straight channels, it is readily applicable to other geometries with seeded cells. The developed simulation can provide useful insights to optimize the mass transport of 3D vascularized porous scaffolds.

REFERENCES:

1. S. J. Hollister, Porous scaffold design for tissue engineering. Nat. Mater. 4, 518 (2005).
2. S. Zhang, et al., A review on the use of computational methods to characterize, design, and optimize tissue engineering scaffolds, with a potential in 3D printing fabrication. Journal of Biomedical Materials Research Part B: Applied Biomaterials 107B, 1329-1351 (2018).
3. B. Grigoryan et al., Multivascular networks and functional intravascular topologies within biocompatible hydrogels. Science 364, 458-464 (2019).